INTERNATIONAL JOURNAL FOR NUMERICAL METHODS IN FLUIDS
Int. J. Numer. Meth. Fluids 2008; **56**:687–702
Published online 27 June 2007 in Wiley InterScience (www.interscience.wiley.com). DOI: 10.1002/fld.1548

Instability of the separated shear layer in flow past a cylinder: Forced excitation

Sanjay Mittal*, †

Department of Aerospace Engineering, Indian Institute of Technology Kanpur, UP 208 016, India

SUMMARY

The receptivity of the separated shear layer for $Re = 300$ flow past a cylinder is investigated by forced excitation *via* an unsteady inflow. In order to isolate the shear layer instability, a numerical experiment is set up that suppresses the primary wake instability. Computations are carried out for one half of the cylinder, in two dimensions. The flow past half a cylinder with steady inflow is found to be stable for $Re = 300$. However, an inlet flow with pulsatile perturbations, of amplitude 1% of the mean, results in the excitation of the shear layer mode. The frequency of the perturbation of the inlet flow determines the frequency associated with the shear layer vortices. For a certain range of forced frequencies the recirculation region undergoes a low-frequency longitudinal contraction and expansion. An attempt is made to relate this instability to a global mode of the wake determined from a linear stability analysis. Interestingly, this phenomenon disappears when the outflow boundary of the computational domain is shifted sufficiently downstream. This study demonstrates the need of carefully investigating the effect of the location of outflow boundaries if the computational results indicate the presence of low-frequency fluctuations. The effect of Re and amplitude of unsteadiness at the inlet are also presented. All computations have been carried out using a stabilized finite element formulation of the incompressible flow equations. Copyright © 2007 John Wiley & Sons, Ltd.

Received 31 May 2006; Revised 14 May 2007; Accepted 15 May 2007

KEY WORDS: shear layer instability; unsteady inflow; circular cylinder; finite element method

1. INTRODUCTION

The flow past a cylinder is associated with various instabilities [1, 2]. The primary instability of the wake sets in at $Re \sim 47$ and eventually leads to the von Karman vortex shedding. The Reynolds number is defined as $Re = \rho U D/\mu$, where ρ is the fluid density, U is the free-stream

*Correspondence to: Sanjay Mittal, Department of Aerospace Engineering, Indian Institute of Technology Kanpur, UP 208 016, India.
†E-mail: smittal@iitk.ac.in

Contract/grant sponsor: Department of Science and Technology, India

speed, D is the diameter of the cylinder and μ is the coefficient of viscosity of the fluid. Beyond $Re \sim 190$ the wake undergoes three-dimensional transitions [1]. At higher Re, instability of the separated shear layer due to the Kelvin–Helmholtz mechanism is observed. Various values of the critical Reynolds number (Re_c), at which this instability is first observed, have been reported in the literature. Bloor [3] observed the shear layer instability for Re larger than 1300. Gerrard [4] observed the shear layer instability at $Re = 350$ and higher. Unal and Rockwell [5] reported that they were unable to observe shear layer transition waves for $Re < 1900$ using flow visualization. Prasad and Williamson [6] found that the end conditions determine the Re_c; it is ~ 1200 for parallel shedding conditions and significantly higher (~ 2600) for the end conditions that result in oblique shedding. They observed that the shear layer fluctuations are intermittent and become stronger with increase in Re. They attributed the intermittent behaviour of these fluctuations to the streamwise movement of the transition point in the shear layer. The observation of the transition waves for $Re \sim 350$ by Gerrard [4] remains unexplained to this date.

The present work is an effort to investigate the possibility of observing the shear layer fluctuations at low Re. At low Re, the shear layer transition waves are very weak and the flow is dominated by the primary instability of the wake. A computational experiment is designed that results in suppression of the primary wake instability but does not annihilate the instability of the separated shear layer. This may, therefore, allow one to observe the shear layer vortices even at low Re.

In an earlier work [7] it was reported that a 'slip' splitter plate occupying a certain portion of the centre-line downstream of the cylinder results in complete suppression of vortex shedding for low Re. For $Re = 100$ a plate of length $2D$ (D is the diameter of the cylinder), whose leading edge is located at $2.68D$ from the centre of the cylinder, is sufficient to completely suppress the vortex shedding. The location and length of the slip plate required to suppress the shedding are functions of the Reynolds number. It is found that for such low Re, similar suppression of vortex shedding can also be achieved by replacing the slip splitter plate with a streamline, i.e. by imposing a no-normal-flow across that part of the wake centre line. This, however, works only for Re lower than ~ 250. It was found [8] that, for the $Re = 300$ flow, even when the entire centre-line downstream of the cylinder is forced to be a streamline, i.e. there is no-normal-flow across the centreline, the wake instability develops and also excites the shear layer mode. It was also found that the $Re = 300$ flow past half a cylinder, with symmetry conditions at the wake centre-line, is stable. Further, it was found that when a secondary cylinder with one-fifth the diameter of the half cylinder is placed close to it, the vortex shedding from the smaller cylinder leads to instability of the separated shear layer of the half cylinder. This instability is periodic but intermittent in nature. These results suggest that although the separated shear layer is linearly stable for the $Re = 300$ flow with a steady inflow, the shear layer mode can be excited by other external disturbances.

The objective of the present work is to further explore the possibility of exciting the shear layer mode for the $Re = 300$ flow. The excitation is provided by a pulsatile perturbation of the inlet flow at certain frequencies. It offers the possibility to answer a few questions: Can the forced oscillations lead to the instability of the separated shear layer? What is the effect of varying the frequency of the excitation? Is there an intrinsic frequency associated with the shear layer instability that is independent of the excitation frequency? It is well known that the $Re = 300$ flow past a cylinder is associated with three-dimensional instabilities. However, the objective of the present work is restricted to studying the instability of the separated shear layer. This instability, along the span of the cylinder, is known to be by and large two-dimensional [1, 9].

The incompressible flow equations, in the velocity pressure form, are solved *via* a stabilized finite element method. The stabilized formulation is based on the SUPG (Streamline-Upwind/

DOI: 10.1002/fld

Petrov–Galerkin) and PSPG (Pressure-Stabilizing/Petrov–Galerkin) stabilization techniques [10]. Several element-level integrals are added to the Galerkin formulation to stabilize the computations against spurious numerical oscillations. The basic Galerkin formulation is unstable for convection-dominated flows and does not allow one to use equal-order-interpolation velocity–pressure elements. The time integration of the governing flow equations is done *via* an implicit procedure that is second-order accurate. The time steps are chosen to adequately resolve the time scales in the physical phenomena. The large-scale coupled non-linear equation systems resulting from the finite element discretization of the governing equations are solved iteratively by employing the GMRES (Generalized Minimal RESidual) procedure in conjunction with diagonal preconditioners. More information on the formulation and its application to computing flows past cylinders can be found in our earlier papers [11–14].

2. THE GOVERNING EQUATIONS

2.1. The incompressible flow equations

Let $\Omega \subset \mathbb{R}^{n_{\mathrm{sd}}}$ and $(0, T)$ be the spatial and temporal domains, respectively, where n_{sd} is the number of space dimensions, and let Γ denote the boundary of Ω. The spatial and temporal coordinates are denoted by $\mathbf{x}$ and t. The Navier–Stokes equations governing incompressible fluid flow are

$$\rho\left(\frac{\partial \mathbf{u}}{\partial t} + \mathbf{u}\cdot\nabla\mathbf{u} - \mathbf{f}\right) - \nabla\cdot\boldsymbol{\sigma} = \mathbf{0} \quad \text{on } \Omega\times(0,T) \tag{1}$$

$$\nabla\cdot\mathbf{u} = 0 \quad \text{on } \Omega\times(0,T) \tag{2}$$

Here ρ, $\mathbf{u}$, $\mathbf{f}$ and $\boldsymbol{\sigma}$ are the density, velocity, body force and the stress tensor, respectively. The stress tensor is written as the sum of its isotropic and deviatoric parts:

$$\boldsymbol{\sigma} = -p\mathbf{I} + \mathbf{T}, \quad \mathbf{T} = 2\mu\boldsymbol{\varepsilon}(\mathbf{u}), \quad \boldsymbol{\varepsilon}(\mathbf{u}) = \tfrac{1}{2}((\nabla\mathbf{u}) + (\nabla\mathbf{u})^{\mathrm{T}}) \tag{3}$$

where p and μ are the pressure and coefficient of dynamic viscosity, respectively.

2.2. Problem set up and boundary conditions

The computational domain is a rectangle with a half circular hole whose diameter lies along the lower edge of the domain. A schematic of the problem set up is shown in Figure 1. The lateral and the downstream boundaries are located at a distance of $50D$ from the centre of the cylinder. The distance between the centre of the cylinder and the upstream boundary is $25D$. The structure of the mesh is same as used in one of our earlier studies [13]. It consists of two parts: a structured grid close to the cylinder and an unstructured mesh in the remaining domain. The structured mesh allows for having adequate control on the resolution of the flow in the boundary layer. It consists of 100 elements in the circumferential direction. The radial thickness of the first layer of elements on the cylinder boundary is $5\times10^{-4}D$. The unstructured mesh is generated *via* the Delaunay's triangulation technique. A view of the mesh is shown in Figure 2. This kind of a hybrid mesh is useful in handling complex geometries by providing adequate resolution close to the body without requiring the same distribution of grid points in the remaining domain. It leads to significant saving of computational resources as opposed to computations on a structured mesh with similar resolution close to the body.

DOI: 10.1002/fld

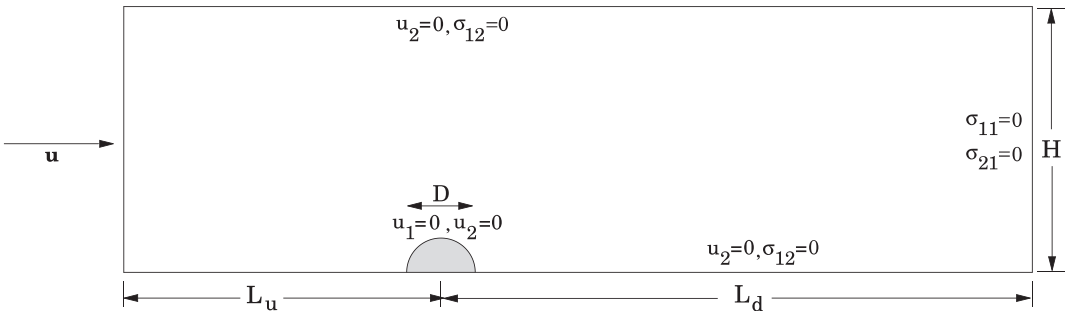

Figure 1. Uniform flow past a cylinder: problem description.

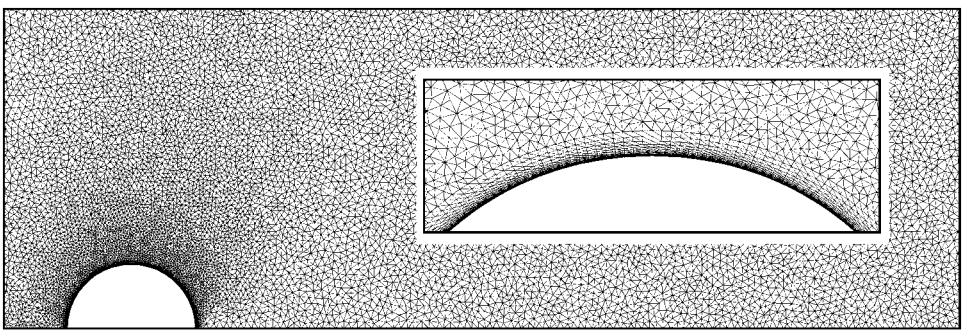

Figure 2. Flow past half cylinder: close-up views of the finite element mesh with 99 014 nodes and 197 164 triangular elements.

The following boundary conditions are applied. At the upstream boundary, the flow speed given by the expression: $U_{\text{mean}}[1 + A\sin(2\pi Ft)]$ is assigned. Here, U_{mean} is the time-averaged speed at the inlet, A is the normalized amplitude of the unsteadiness at inlet, F is the non-dimensional frequency and t is the non-dimensional time. F and t have been non-dimensionalized with respect to U_{mean} and cylinder diameter, D. Another quantity that is useful is the Strouhal number. It represents the vortex shedding frequency non-dimensionalized with respect to D and U_{mean}. At the downstream boundary, a Neumann-type boundary condition for the velocity is specified that corresponds to zero stress vector. On the upper and lower boundaries a 'slip-wall' boundary condition is employed, i.e. the component of velocity normal to and the component of stress vector along this boundary are prescribed zero values. No-slip condition on the velocity is applied on the cylinder surface.

3. THE FINITE ELEMENT FORMULATION

Consider a finite element discretization of Ω into subdomains Ω^e, $e = 1, 2, \ldots, n_{\text{el}}$, where n_{el} is the number of elements. Based on this discretization, for velocity and pressure, we define the finite element trial function spaces $\mathcal{S}^h_{\mathbf{u}}$ and $\mathcal{S}^h_p$, and weighting function spaces $\mathcal{V}^h_{\mathbf{u}}$ and $\mathcal{V}^h_p$.

DOI: 10.1002/fld

These function spaces are selected, by taking the Dirichlet boundary conditions into account, as subsets of $[\mathbf{H}^{1h}(\Omega)]^{n_{\text{sd}}}$ and $\mathbf{H}^{1h}(\Omega)$, where $\mathbf{H}^{1h}(\Omega)$ is the finite-dimensional function space over Ω. The stabilized finite element formulation of Equation (1) is written as follows: find $\mathbf{u}^h \in \mathscr{S}^h_{\mathbf{u}}$ and $p^h \in \mathscr{S}^h_p$ such that $\forall \mathbf{w}^h \in \mathscr{V}^h_{\mathbf{u}}$ and $q^h \in \mathscr{V}^h_p$

$$\int_\Omega \mathbf{w}^h \cdot \rho \left(\frac{\partial \mathbf{u}^h}{\partial t} + \mathbf{u}^h \cdot \boldsymbol{\nabla} \mathbf{u}^h - \mathbf{f} \right) \mathrm{d}\Omega + \int_\Omega \boldsymbol{\varepsilon}(\mathbf{w}^h) : \boldsymbol{\sigma}(p^h, \mathbf{u}^h)\, \mathrm{d}\Omega$$

$$+ \int_\Omega q^h \boldsymbol{\nabla} \cdot \mathbf{u}^h \, \mathrm{d}\Omega + \sum_{e=1}^{n_{\text{el}}} \int_{\Omega^e} \frac{1}{\rho} (\tau_{\text{SUPG}} \rho \mathbf{u}^h \cdot \boldsymbol{\nabla} \mathbf{w}^h + \tau_{\text{PSPG}} \boldsymbol{\nabla} q^h)$$

$$\cdot \left[\rho \left(\frac{\partial \mathbf{u}^h}{\partial t} + \mathbf{u}^h \cdot \boldsymbol{\nabla} \mathbf{u}^h - \mathbf{f} \right) - \boldsymbol{\nabla} \cdot \boldsymbol{\sigma}(p^h, \mathbf{u}^h) \right] \mathrm{d}\Omega^e$$

$$+ \sum_{e=1}^{n_{\text{el}}} \int_{\Omega^e} \tau_{\text{LSIC}} \boldsymbol{\nabla} \cdot \mathbf{w}^h \rho \boldsymbol{\nabla} \cdot \mathbf{u}^h \, \mathrm{d}\Omega^e = \int_{\Gamma_h} \mathbf{w}^h \cdot \mathbf{h}^h \, \mathrm{d}\Gamma \tag{4}$$

In the variational formulation given by Equation (4), the first three terms and the right-hand side constitute the Galerkin formulation of the problem. It is well known that the Galerkin formulation is unstable with respect to the advection operator as the cell Reynolds number (based on the local flow velocity and mesh size) becomes large. Also, not all combinations of velocity and pressure interpolations are admissible in the Galerkin formulation. Elements that do not satisfy the Babuska–Brezzi condition lead to oscillatory solutions and, sometimes, no solution at all. To give stability to the basic formulation, a series of element-level integrals are added. The first series of element-level integrals are the SUPG and PSPG stabilization terms added to the variational formulations [10]. The second series of element-level integrals are stabilization terms based on the least squares of the divergence-free condition on the velocity field. Presently, same definition for τ_{PSPG} and τ_{SUPG} is being used. It is given by the following relation based on the values of τ for the advection and diffusion limits:

$$\tau_{\text{SUPG}} = \tau_{\text{PSPG}} = \left(\frac{1}{\tau^2_{\text{ADV}}} + \frac{1}{\tau^2_{\text{DIF}}} \right)^{-1/2} \tag{5}$$

where

$$\tau_{\text{ADV}} = \frac{h^e}{2\|\mathbf{u}^h\|}, \quad \tau_{\text{DIF}} = \frac{(h^e)^2}{12\nu} \tag{6}$$

Here, h^e is the element length and various definitions have been used by researchers in the past. Mittal [15] conducted a systematic numerical study to investigate the effect of high aspect ratio elements on the performance of the finite element formulation for three commonly used definitions of h. In this work, we use the definition based on the minimum edge length of an element. The coefficient τ_{LSIC} is defined as

$$\tau_{\text{LSIC}} = \left(\frac{1}{\delta^2_{\text{ADV}}} + \frac{1}{\delta^2_{\text{DIF}}} \right)^{-1/2} \tag{7}$$

DOI: 10.1002/fld

where

$$\delta_{\mathrm{ADV}} = \frac{h^e \|\mathbf{u}^h\|}{2}, \quad \delta_{\mathrm{DIF}} = \frac{(h^e)^2 (\|\mathbf{u}^h\|)^2}{12\nu} \tag{8}$$

Both stabilization terms are weighted residuals, and therefore maintain the consistency of the formulation. Other details of the formulation can be found in Tezduyar *et al.* [10]. For a description of alternative definitions of the stabilization coefficients the interested reader may refer to the article by Tezduyar [16].

The time integration of the flow equations is carried out *via* the generalized trapezoidal algorithm. The parameter α in the scheme is chosen to be 0.5. This results in second-order accuracy in time. A time step of 0.025 is utilized for all the computations in this paper. The nonlinear equation system resulting from the finite element discretization of the flow equations is solved using the GMRES technique [17] in conjunction with diagonal preconditioners. The implicit method used in the present work allows us to seek steady-state solutions by simply dropping the unsteady terms from the governing equations and using $\alpha = 1$ in the generalized trapezoidal algorithm.

4. RESULTS

4.1. Steady flow

First, flow past half a cylinder with steady inflow is computed. These computations lead to steady-state solutions for all $Re \leqslant 300$ that were attempted. The solutions obtained by solving the unsteady equations following an impulsive start and the ones by solving the steady-state equations are found to be same. The top frame in Figure 3 shows the steady-state vorticity field for the $Re = 300$ flow. Fornberg [18–20] has presented results for steady flow past a cylinder for Re upto 800 in a series of papers. Recently, Gajjar and Azzam [21] have been able to obtain steady flow solutions for Re as large as 3500. They have also presented a detailed review of the work done on steady flow past bluff bodies. The results from the present computations are in good agreement with published results [18–21]. For example, the steady-state drag coefficient from the present computations for $Re = 100$ flow is 1.065 and the length of the wake bubble, measured from the cylinder centre, is $6.67D$. These values, reported by Fornberg [20] are 1.060 and $6.60D$, respectively. The values reported by Gajjar and Azzam [21], for the case when the lateral boundary is located at $25D$ from the centre of the cylinder, are 1.08 and $6.65D$, respectively. Fornberg [20] and Gajjar and Azzam [21] have shown that, in general, as the lateral boundary is brought closer to the cylinder the drag coefficient increases and the recirculation bubble length decreases. For the $Re = 300$ flow the present computations result in the steady-state drag coefficient of 0.734 and a recirculation bubble length of $20.49D$. The values for the same, reported by Fornberg [20], are 0.726 and $20.40D$, respectively. For more details on the steady-state flow past a cylinder and for the performance of the present algorithm for unsteady flows, the interested reader is referred to our earlier papers [8, 13, 14].

4.2. Linear stability analysis of the $Re = 300$ steady flow

A global linear stability analysis of the non-parallel steady flow is carried out *via* the procedure described in our earlier papers [12, 22]. The unsteady solution, $(\mathbf{u}, p)$, is expressed as a combination

DOI: 10.1002/fld

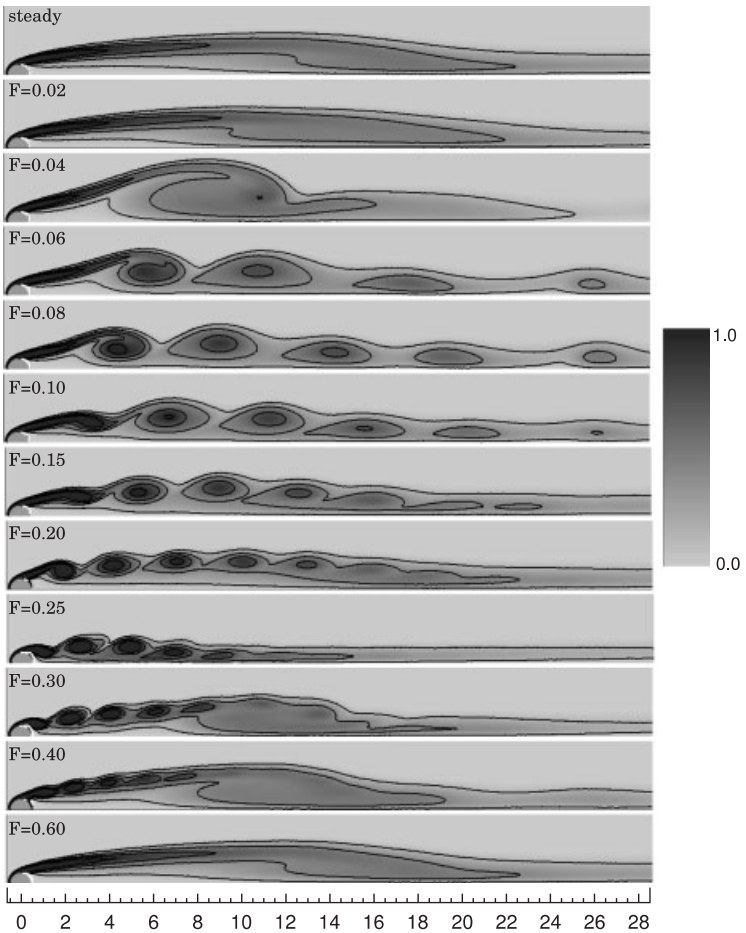

Figure 3. $Re = 300$, $A = 0.01$ flow past half cylinder: vorticity fields for the fully developed flow for various F. The top frame shows the steady-state flow for steady inflow. All the other frames show the instantaneous field for the fully developed periodic flow with unsteady inflow for various F. The colour map for the magnitude of the vorticity is also shown.

of the steady solution and the disturbance: $\mathbf{u} = \mathbf{U} + \mathbf{u}'$ and $p = P + p'$. Here, $\mathbf{U}$ and P represent the steady-state solution whose stability is to be determined while $\mathbf{u}'$ and p' are the perturbation fields of the velocity and pressure, respectively. We further assume that the disturbances are small and of the form $\mathbf{u}'(\mathbf{x}, t) = \hat{\mathbf{u}}(\mathbf{x})e^{\lambda t}$ and $p'(\mathbf{x}, t) = \hat{p}(\mathbf{x})e^{\lambda t}$. Substituting these forms of the perturbations in the governing equations (Equations (1)–(2)) and subtracting from them, the equations for steady flow, one obtains a generalized eigenvalue problem. λ is the eigenvalue of the fluid system and governs its stability. In general, $\lambda = \lambda_r + i\lambda_i$ where, λ_r and λ_i are the real and imaginary parts, respectively. The steady-state solution $(\mathbf{U}, P)$ is associated with a global unstable mode if the corresponding eigenvalue has a positive real part.

The linear stability analysis for the $Re = 300$ flow past a cylinder with steady inflow shows that all the global modes associated with this flow are stable. The most unstable eigenmode

DOI: 10.1002/fld

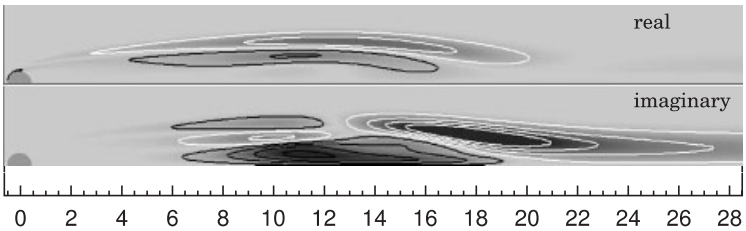

Figure 4. $Re = 300$ flow past half cylinder with steady inflow: vorticity field for the real and imaginary parts of the most unstable eigenmode.

is the one whose eigenvalue has the largest real part. The vorticity fields for the real and imaginary parts of the most unstable eigenmode are shown in Figure 4. The growth rate, λ_r, for this mode is -0.4377×10^{-2} while the Strouhal number associated with it is ~ 0.001. This is a very low-frequency mode compared to the usual wake mode responsible for vortex shedding. The eigenfunctions are normalized such that their Euclidean norm is unity.

To understand the dynamics associated with this mode, we construct a time-dependent flow by adding the eigenmode to the steady-state solution, i.e. $\mathbf{U}(\mathbf{x}) + \hat{\mathbf{u}}(\mathbf{x})e^{\lambda t}$ and $P(\mathbf{x}) + \hat{p}(\mathbf{x})e^{\lambda t}$. To enhance the visual effect, the growth rate is made positive; the original value of λ_r is replaced with a small but positive value: 6.0×10^{-4}. The resulting solution for one cycle of the global mode is shown in Figure 5. From the figure it is seen that this global mode associated with the wake of the cylinder corresponds to the expansion and contraction of the recirculation bubble. Of course, in the real flow it is stable for $Re = 300$. However, it may still be observed if it were to be excited either by non-linear interactions with other global modes or *via* external inputs to the flow. To the best of our knowledge this mode has never been reported before in the context of flow past a cylinder.

4.3. Flow for unsteady inlet, $A = 0.01$, $Re = 300$

Figure 3 shows the instantaneous vorticity fields for the $Re = 300$ flow past half a cylinder with an unsteady inlet velocity for various excitation frequencies. In all cases, the amplitude of the unsteady component of the inlet flow speed is 1% of the time-averaged speed ($A = 0.01$). The vorticity field for a steady inflow is also shown in the top frame of Figure 3. In all other cases, the pictures shown are for the fully developed unsteady flow following an impulsive start. Throughout this paper, the magnitude of a flow quantity is displayed in grey scale: darker the shade, larger is the magnitude. White contour lines indicate a positive value while the black ones represent negative value. The frames corresponding to $F = 0.02$ and 0.60 appear to be quite similar to that for the steady-state flow. For all other excitation frequencies studied, the unsteadiness in the flow due to the instability of the shear layer can be readily observed. The size of the shear layer vortices and their spacing vary with the excitation frequency. While the vortices are large for low values of F, they are smaller and spaced closer to each other for higher values of F. Time histories of the flow quantities for probes placed at various locations in the wake indicate that in each case the dominant frequency of the unsteadiness corresponds to the excitation frequency. Figure 6 shows one such set of time histories of the y component of velocity at a point located at $(2.5D, 1.0D)$ with respect to the centre of the cylinder. This shows that, at least at the low Re, the frequency associated with the shear layer instability is determined largely by the excitation frequency.

DOI: 10.1002/fld

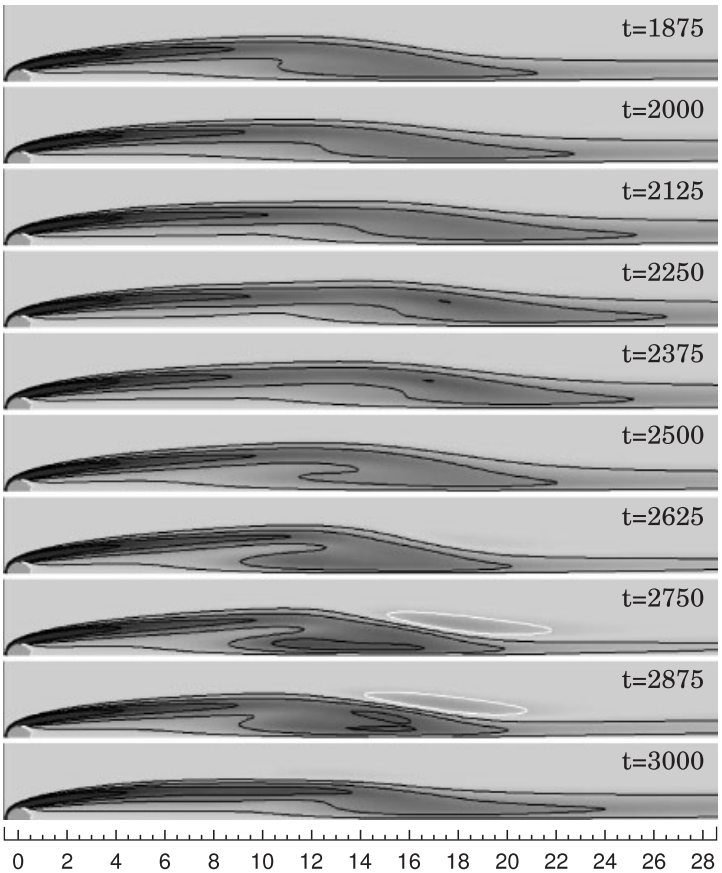

Figure 5. $Re = 300$ flow past half cylinder with steady inflow: vorticity field during one period of wake oscillation simulated by taking a linear combination of the steady-state solution and the most unstable eigenmode. The colour map for the vorticity field is the same as shown in Figure 3.

It appears that the separated shear layer is convectively unstable and the unsteadiness at the inlet is able to excite these shear layer modes.

From Figure 6 it is seen that the flow excitations in the near wake first increase with increase in F and then decrease with further increase in F. The maximum oscillation amplitude is realized for $F \sim 0.25$. This observation correlates well with the vorticity fields shown in Figure 3. For low values of F ($\leqslant 0.25$) the excitation affects the structure of the recirculation bubble quite significantly. However, for larger values of F ($\geqslant 0.30$) the size of the recirculation zone is quite similar to that for the steady flow. To view the effect of F in more detail we subtract from the unsteady flow the steady-state flow and show the resulting perturbation field of the vorticity in Figure 7. The shear layer vortices can now be clearly observed for all values of F. The perturbations in the vorticity field, with respect to the steady flow, are largest for $F = 0.25$. As is also seen from Figure 6, the strength of the vortices reduces as F is increased beyond 0.25. At $F = 0.60$, the vortices are very weak and confined to the very near wake of the cylinder. Consequently, the flow for $F = 0.60$ is very similar to the flow with steady inflow.

DOI: 10.1002/fld

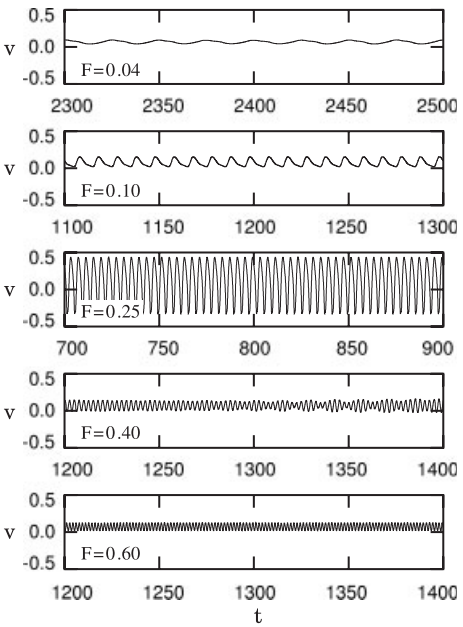

Figure 6. $Re = 300$, $A = 0.01$ flow past half cylinder with unsteady inflow: time histories of the vertical velocity at a point located at $(2.5D, 1.0D)$ with respect to the centre of the cylinder, for various values of F.

4.3.1. A low-frequency wake instability. An interesting phenomenon is observed for $F = 0.30$ and 0.40. While the shear layer vortices are not too strong to alter the basic structure of the recirculation bubble observed for the steady inflow, they are still strong enough not to get completely diffused by the time they reach the far downstream end of the recirculation bubble. Consequently, they are convected back towards the cylinder by the recirculating flow. This can be noticed from the perturbations in the vorticity field shown in Figure 7. The interaction between the recirculating bubble, the separated shear layer and the shear layer vortices leads to an additional instability that involves a cyclic contraction and expansion of the recirculation bubble and an intermittent intensification of the formation of shear layer vortices. This is reminiscent of the low-frequency wake mode for the steady inflow that was described in the previous section (see Figures 4 and 5). A possible reason for the excitation of this mode could be the non-linear interaction between the wake mode and the shear layer vortices. Another observation that supports this possibility is the low frequency associated with the instability in the two flows.

The time history of the vertical velocity at a point $(15D, 2D)$ with respect to the centre of the cylinder, for $F = 0.40$, is shown in Figure 8. Also shown in the same figure are the instantaneous vorticity fields at certain time instants during one period of the contraction and expansion of the recirculation bubble. The oscillation frequency of the recirculation bubble is very low: ~ 0.0025. However, it is larger than the frequency for the wake mode for the flow with steady inflow. The difference between the two frequencies may be attributed to the non-linear effects that are known to alter the frequencies predicted by linear theories. During the longitudinal contraction of the recirculation bubble, stronger shear layer vortices are formed. This results in larger amplitude

DOI: 10.1002/fld

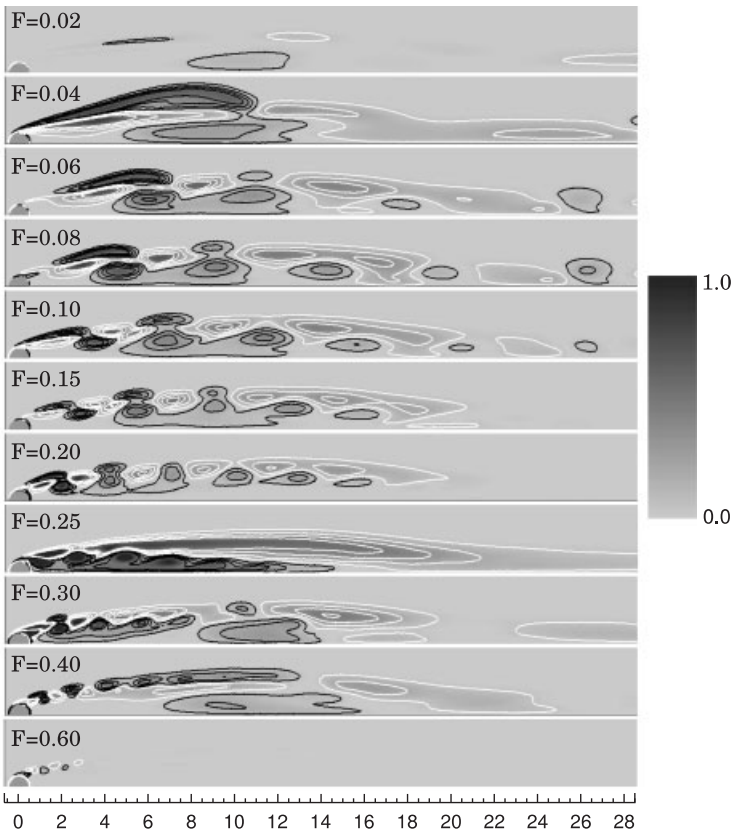

Figure 7. $Re = 300$, $A = 0.01$ flow past half cylinder with unsteady inflow: perturbations in the vorticity field, with respect to the steady flow, for various F. The colour map is also shown. There are nine equispaced contour lines between ± 0.5. The white contour lines represent positive values while the black ones represent negative values.

oscillations in the velocity field as is seen from the time history shown in Figure 8. This behaviour is very similar to the one observed in our earlier work [8] where the separated shear layer for a steady inflow is excited by a smaller secondary cylinder.

To investigate further this low-frequency instability, we carry out computations for various locations of the outflow boundary, L_d. Figure 9 shows the time history of the vertical velocity at a point $(15D, 2D)$ with respect to the centre of the cylinder for $F = 0.40$ and with various values of L_d. It is seen that although the shear layer instability is quite similar in all the cases, the low-frequency instability becomes weaker as the outflow boundary moves downstream. For L_d in excess of $150D$ the wake instability is completely eliminated. The solutions for values of L_d larger than $150D$ are virtually identical. Figure 10 shows the instantaneous vorticity field computed using a domain with $L_d = 250D$ for the fully developed flow. The solution at all times appears very similar to the one shown in the figure. The shear layer vortices are clearly observed. However, wake instability corresponding to the streamwise pulsation of the recirculation zone is absent in this solution. This observation points to the low-frequency instability being a numerical artefact

DOI: 10.1002/fld

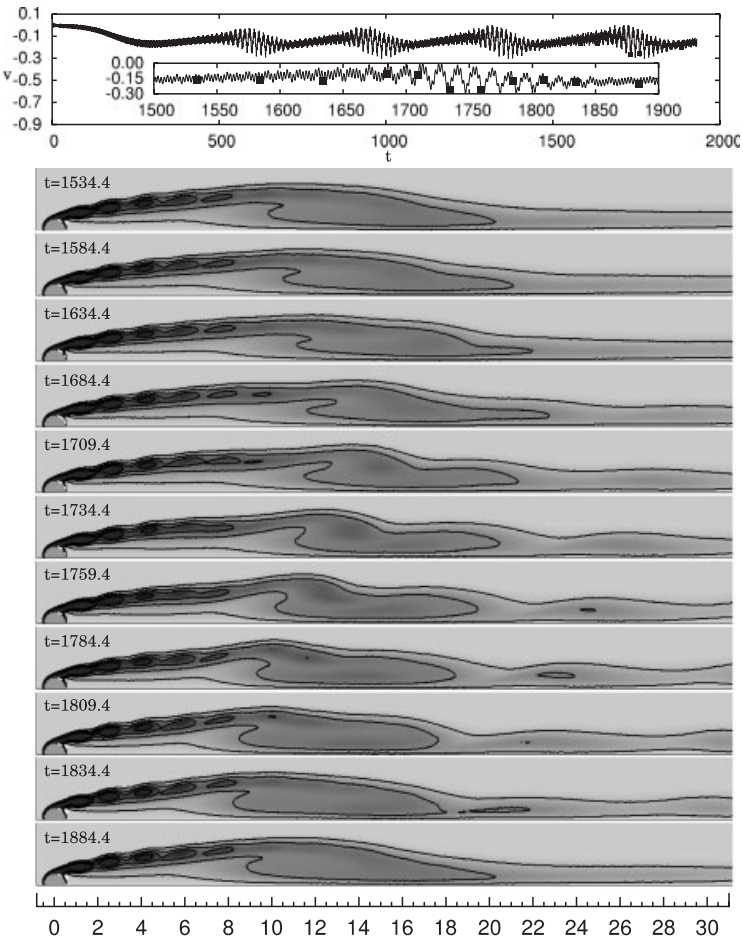

Figure 8. $Re = 300$, $F = 0.40$ flow past half cylinder with unsteady inflow: time history of the vertical velocity at a point located at $(15D, 2D)$ with respect to the centre of the cylinder and the vorticity fields at certain time instants during, approximately, one period of the contraction and expansion of the recirculation bubble. The colour map for the vorticity field is the same as shown in Figure 3.

that disappears when the outflow boundary is sufficiently far away. This study clearly demonstrates the need to be very careful in choosing the location of boundaries in such computations. It appears that if the outflow boundary is not sufficiently far away from the bluff body, the low-frequency wake instability can be excited. As expected, the computations for lower values of F (for example, $F = 0.2$) do not show any significant differences for various locations of the outflow boundary.

4.4. Effect of the amplitude of unsteadiness at inlet; $Re = 300$, $F = 0.2$

The effect of A, amplitude of unsteadiness at the inlet, is studied for the $Re = 300$ and $F = 0.2$ flow. Results for three values of A are presented. The vorticity fields for the fully developed unsteady solutions are shown in Figure 11 while the time histories of the vertical velocity at $(15D, 2D)$

DOI: 10.1002/fld

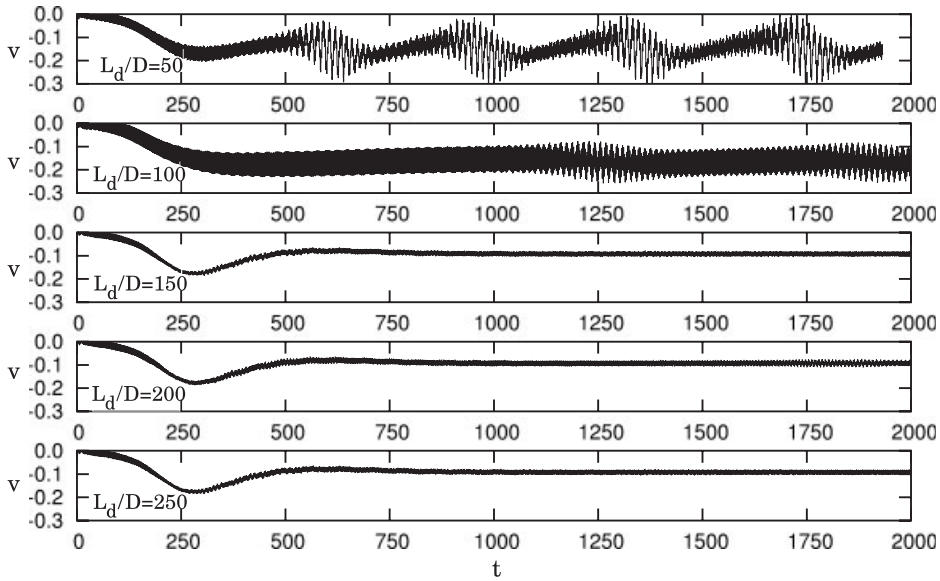

Figure 9. $Re = 300$, $F = 0.40$ flow past half cylinder with unsteady inflow: time history of the vertical velocity at a point located at $(15D, 2D)$ with respect to the centre of the cylinder for various locations of the outflow boundary.

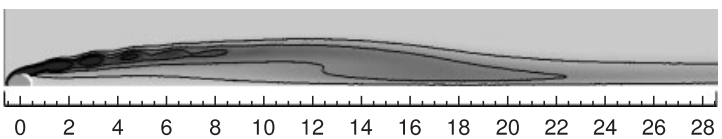

Figure 10. $Re = 300$, $F = 0.40$ flow past half cylinder computed on a domain with $L_d = 250D$: vorticity field for the fully developed unsteady flow. The colour map for the vorticity field is the same as shown in Figure 3.

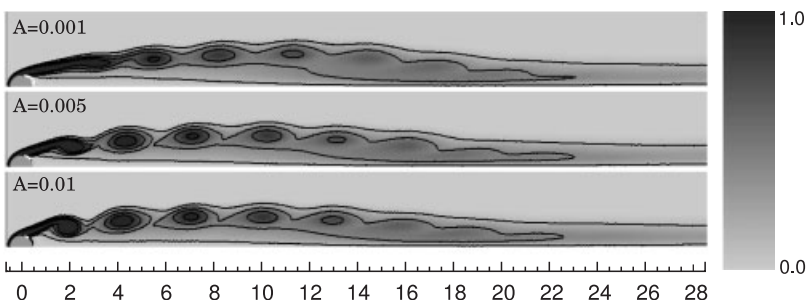

Figure 11. $Re = 300$, $F = 0.20$ flow past half cylinder: vorticity fields for the fully developed unsteady flow for various values of A. The colour map for the magnitude of the vorticity is also shown.

DOI: 10.1002/fld

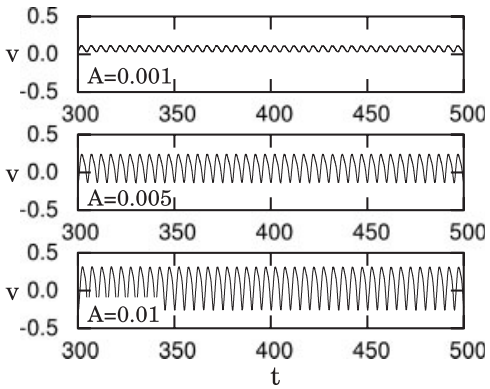

Figure 12. $Re = 300$, $F = 0.20$ flow past half cylinder: time histories of the vertical velocity at a point located at $(2.5D, 1.0D)$ with respect to the centre of the cylinder, for various values of A.

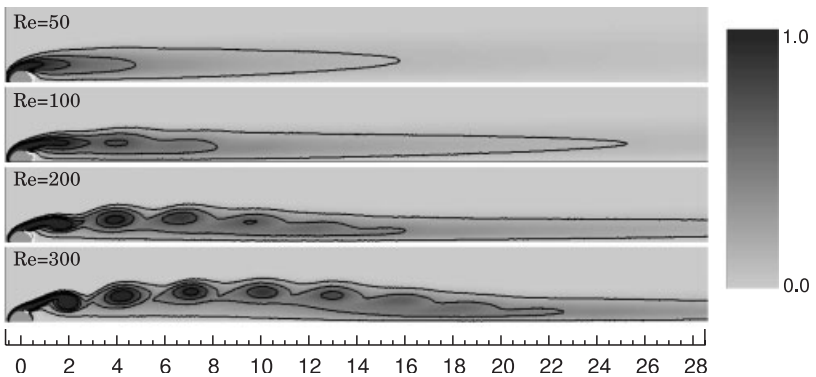

Figure 13. $A = 0.01$, $F = 0.20$ flow past half cylinder: vorticity fields for the fully developed unsteady flow for various Re. The colour map for the magnitude of the vorticity is also shown.

are shown in Figure 12. Qualitatively, the behaviour in all the three cases is quite similar. The strength of the shear layer vortices, as suggested by the amplitude of the vertical velocity at $(15D, 2D)$ increases with A. The amplitude of the vertical velocity is 0.07814 for $A = 0.001$, 0.37411 for $A = 0.005$ and 0.30926 for $A = 0.01$. The variation of the amplitude, for these values of A, is already deviating from being linear with A. It is expected that for larger values of A the response of the flow might be quite different. The shear layer modes, as they become stronger, might excite other modes of the flow.

4.5. Effect of Re; $A = 0.01$, $F = 0.2$

Figure 13 shows the vorticity fields for the fully developed unsteady solution for $Re = 50$, 100, 200 and 300 for $A = 0.01$ and $F = 0.2$. The time histories of the vertical velocity at $(15D, 2D)$ are shown in Figure 14. The shear layer vortices are not observed for $Re = 50$ and are very weak

DOI: 10.1002/fld

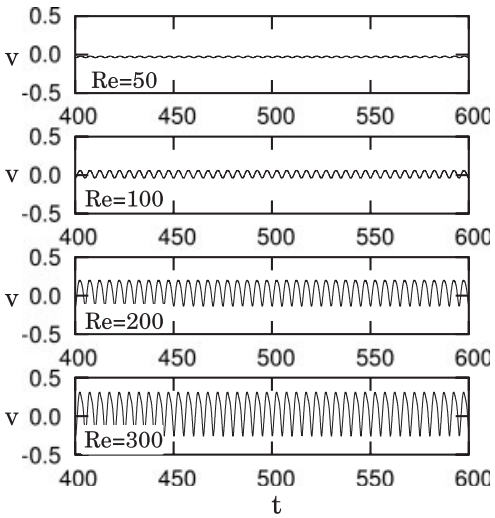

Figure 14. $A = 0.01$, $F = 0.20$ flow past half cylinder: time histories of the vertical velocity at a point located at $(2.5D, 1.0D)$ with respect to the centre of the cylinder, for various values of Re.

for $Re = 100$. The strength increases with increase in Re. Almost a linear increase in amplitude of the disturbance is observed between $Re = 100$ and 300. In all the cases the time variation of the frequency of shedding of the shear layer vortices is 0.2.

5. CONCLUSIONS

It is shown that, although the shear layer for $Re = 300$ flow past a cylinder with steady inflow is stable, it is possible to excite the shear layer mode at these low Re *via* external disturbances in a certain range of frequencies. The frequency of the formation and shedding of shear layer vortices is determined by the excitation frequency. For $F = 0.2$ and $A = 0.01$ shear layer vortices can be observed at Re as low as 100. In certain cases, the shear layer instability is accompanied by a low-frequency longitudinal oscillation of the recirculation bubble. This low-frequency oscillation has been identified to be caused by a wake mode. The wake mode has been obtained *via* a global linear stability analysis of the flow equations. However, the wake instability disappears when the outflow boundary is located in excess of 150 diameters away from the cylinder. This study demonstrates the need of carefully investigating the effect of location of outflow boundaries if the computational results indicate the presence of low-frequency fluctuations.

ACKNOWLEDGEMENT

Partial support for this work from the Department of Science and Technology, India is gratefully acknowledged.

DOI: 10.1002/fld

REFERENCES

1. Williamson CHK. Vortex dynamics in the cylinder wake. *Annual Review of Fluid Mechanics* 1996; **28**:477–539.
2. Roshko A. Perspectives on bluff body aerodynamics. *Journal of Wind Engineering and Industrial Aerodynamics* 1993; **49**:79–100.
3. Bloor MS. The transition to turbulence in the wake of a circular cylinder. *Journal of Fluid Mechanics* 1964; **19**:290–304.
4. Gerrard JH. The wakes of cylindrical bluff bodies at low Reynolds number. *Philosophical Transactions of the Royal Society of London*, *Series A* 1978; **288**:351–382.
5. Unal MF, Rockwell D. On the vortex formation from a cylinder. Part 1. The initial instability. *Journal of Fluid Mechanics* 1988; **190**:491–512.
6. Prasad A, Williamson CHK. The instability of the shear layer separating from a bluff body. *Journal of Fluid Mechanics* 1997; **333**:375–402.
7. Mittal S. Effect of a 'slip' splitter plate on vortex shedding from a cylinder. *Physics of Fluids* 2003; **15**:817–820.
8. Mittal S. Excitation of shear layer instability in flow past a cylinder at low Reynolds number. *International Journal for Numerical Methods in Fluids* 2005; **49**:1147–1167.
9. Braza M, Chassaing P, Ha Minh H. Prediction of large-scale transition features in the wake of a circular cylinder. *Physics of Fluids A* 1990; **2**:1461–1471.
10. Tezduyar TE, Mittal S, Ray SE, Shih R. Incompressible flow computations with stabilized bilinear and linear equal-order-interpolation velocity–pressure elements. *Computer Methods in Applied Mechanics and Engineering* 1992; **95**:221–242.
11. Mittal S. Computation of 3D flows past circular cylinders of low aspect ratio. *Physics of Fluids* 2001; **13**:177–191.
12. Mittal S, Kumar B. Flow past a rotating cylinder. *Journal of Fluid Mechanics* 2003; **476**:303–334.
13. Singh SP, Mittal S. Flow past a cylinder: shear layer instability and drag crisis. *International Journal for Numerical Methods in Fluids* 2005; **47**:75–98.
14. Mittal S, Singh S. Vortex induced vibrations at subcritical *Re*. *Journal of Fluid Mechanics* 2005; **534**:185–194.
15. Mittal S. On the performance of high aspect-ratio elements for incompressible flows. *Computer Methods in Applied Mechanics and Engineering* 2000; **188**:269–287.
16. Tezduyar TE. Computation of moving boundaries and interfaces and stabilization parameters. *International Journal for Numerical Methods in Fluids* 2003; **43**:555–575.
17. Saad Y, Schultz M. GMRES: a generalized minimal residual algorithm for solving nonsymmetric linear systems. *SIAM Journal on Scientific and Statistical Computing* 1986; **7**:856–869.
18. Fornberg B. A numerical study of steady viscous flow past a circular cylinder. *Journal of Fluid Mechanics* 1980; **98**:819–855.
19. Fornberg B. Steady viscous flow past a circular cylinder up to Reynolds number 600. *Journal of Computational Physics* 1985; **98**:297–320.
20. Fornberg B. Steady incompressible flow past a row of circular cylinders. *Journal of Fluid Mechanics* 1991; **225**:655–671.
21. Gajjar JSB, Azzam NA. Numerical solution of the Navier–Stokes equations for the flow in a cylinder cascade. *Journal of Fluid Mechanics* 2004; **520**:51–82.
22. Kumar B, Mittal S. Effect of blockage on critical parameters for flow past a circular cylinder at low Reynolds number. *International Journal for Numerical Methods in Fluids* 2006; **50**:987–1001.

DOI: 10.1002/fld